J Mater Sci (2016) 51:9879–9888

Post annealing temperature-dependent morphological and electrochemical properties of copper hydroxide thin film electrodes obtained by anodization of copper

T. S. Ghadge[1] and B. J. Lokhande[1,*]

[1] School of Physical Sciences, Solapur University, Solapur, MS 413 255, India

Received: 4 April 2016
Accepted: 12 July 2016
Published online: 20 July 2016

ABSTRACT

Anodization of copper substrates was made in 1 M aqueous sodium hydroxide solution to prepare copper hydroxide thin films. The prepared samples (at 0.9 V) were annealed in air for 1 h by varying the annealing temperature from 523 to 673 K. XRD study confirms the orthorhombic crystal structure for copper hydroxide, whereas cubic to monoclinic crystal structure transformation was observed for copper oxide with increasing annealing temperature. The increase in granular size of copper oxide with temperature was clearly endorsed from morphological study. Electrochemical study reveals the pseudocapacitive behavior for the sample annealed at 598 K with optimum-specific capacitance of 6000 F/g at the scan rate 2 mV/s in 1 M NaOH. The Specific energy, Specific power, and Columbic efficiency (η) were calculated by using chronopotentiometric technique. Electrochemical impedance spectroscopy carried out in the frequency range of 1 mHz–1 MHz gives internal resistance which is about 1.75 Ω/cm^2. The Randles equivalent circuit and its circuitry parameters are reported.

Introduction

Electrochemical capacitors (EC's) (or supercapacitors or ultracapacitors or pseudocapacitors) are the capacitor, having high power density, high energy density, and long cycle life as compared to electrostatic capacitors [1]. In EC's, charges stored in between electrode and electrolyte interface, hence electrochemical mechanism of energy storage gives new system of charge storage and carries the more charges as compared to electrostatic capacitor. The EC's are classified in two types depending on charge storage mechanisms such as (1) electric double-layer capacitors in which charge separation occurs at electrode–electrolyte interface [2, 3]—E.g., electrodes of carbon nanotubes (CNT's), activated carbon, and graphene [4], and (2) pseudocapacitor, where charge separation takes place at the surface of electrode—E.g., electrodes of conducting polymers and transition metal oxides [5–9]. For the improvement of capacitance of supercapacitor, ruthenium oxide is the most studied material [10, 11] formed by sol–gel and electrodeposition reporting large SC 720 and 788 F/g, respectively, with excellent reversibility [11, 12]. Because of highly

Address correspondence to E-mail: bjlokhande@yahoo.com

DOI 10.1007/s10853-016-0221-0

poisonous nature and high cost of ruthenium, alternative materials to ruthenium oxide were tried. The other electrode materials like Fe_2O_3 [13], Co_3O_4 [14], NiO [15, 16], MoO_2 [17], MnO_2 [18, 19], and CuO [20] shows good response to electrochemical performance. Out of these electrode materials, copper oxide is found to be cost effective, easy to prepare, and non-toxic. Copper oxide shows different nanosized dimensions such as, nanospheres, nanoflowers, nanorods, and nanotubes. In rechargeable Li^+ ion batteries, the capacity for Li^+ storage depends upon the shape and structure of the nanosized copper oxide [21]. The low cost of CuO electrode futurizes better potential application for supercapacitor and also alternative for high-cost materials. Anodization of metals is a simple and well-established technique to form highly self-ordered metal oxide nanostructures [22]. Anodization was widely used in making different nanostructures of several metal hydroxides/oxides [23, 24]. Anodized $Cu(OH)_2$ thin films of nanoneedle-type morphology with 115 F/gm SC in 1 M NaOH have been reported by Jadhav et al. [25]. Zhang et al. and Wen et al. reported the synthesis of $Cu(OH)_2$ nanoribbons and nanotubes in a single-crystal form by using a process of surface oxidation of copper foil in alkaline solution [26, 27]. Patake et al. reported the formation of electrodeposited porous and amorphous copper oxide thin films from alkaline sulfate bath. The prepared electrode shows 36 F/g SC in 1 M Na_2SO_4 [28]. Shaikh et al. reported the synthesis of CuO–PAA hybrid thin films by a spin coating technique. Coated films were annealed at different annealing temperatures such as 300, 400, and 500 °C. The obtained values of SC increase from 41 to 136 F/g carried in 1 M H_2SO_4 [29], which clearly indicates post annealing temperature dependent of the electrochemical properties of the electrode materials.

Herein, the attempt was made for the preparation of copper hydroxide thin films by anodization of copper at various anodic potentials. Also, the copper oxide was obtained from post annealing treatment at various temperatures on the deposited copper hydroxide thin films. The formation mechanism of copper hydroxide thin films from anodization of copper is discussed briefly and also a systematic investigation on the post annealing temperature-dependent structural, morphological, and electrochemical properties is successfully done.

Experimental

The anodization setup includes, the two-electrode systems in which copper substrate (1.1 cm^2) acting as a working electrode at anode and platinum wire acts as a counter electrode at cathode. Deposition was carried in 10 ml, 1 M NaOH electrolyte. Thin film samples of copper hydroxide were obtained by varying the deposition potential as 0.1, 0.5, 0.9, 1.1, and 1.3 V for the period of 30 min (the deposited samples were denoted as D_1, D_2, D_3, D_4, and D_5, respectively). On the basis of capacitive nature and adherency, sample gets optimized. The optimized copper hydroxide samples (deposited at 0.9 V, for 30 min) get annealed separately in air for 1 h by varying the temperatures as 523, 548, 573, 598, 623, and 673 K to get copper oxide thin films. The annealed samples were further denoted as T_1, T_2, T_3, T_4, T_5, and T_6, respectively. Weight of all deposited samples (mg/cm^2) was measured by gravimetric weight difference method which is about ~0.1 mg/cm^2. The internal geometry and crystal parameters of all samples were analyzed by using X-ray diffraction patterns carried out by X-ray diffractometer (XRD) (Rigaku D/max2550Vb +18 kw with CuKα, $\lambda = 1.54056$ Å) in the range of diffraction angle 2θ from 20° to 80°. Surface morphology was observed using a scanning electron microscope (SEM) JEOLJSM-6360. The electrochemical properties of all prepared samples were carried out using computer-controlled potentiostat (CHI 600AD—electrochemical analyzer/workstation, CH instruments, USA) with standard three-electrode cell having platinum wire as a counter electrode and saturated Ag/AgCl as a reference electrode.

Results and discussion

Initially, there is a formation of $Cu(OH)_2$; after annealing it gets converted into Cu_2O and then CuO. The phase transition occurs due to the change in +2 to +1 oxidation state and vice versa [28]. The possible reactions at anode to form copper hydroxide and then formation of copper oxide (I) are given as

$$Cu \rightarrow 2e^- + Cu^{2+}$$

$$Cu^{2+} + 2OH^- \rightarrow Cu(OH)_2$$

$$4Cu(OH)_2 \xrightarrow{\Delta} 2Cu_2O + 4H_2O\uparrow + O_2\uparrow$$

Table 1 Variation of *C* and SC for the samples carried at different deposition potentials (a) and temperatures (b)

Sample	C (F)	SC (F/g)
(a)		
D_1 (0.1 V)	0.118	107.2
D_2 (0.5 V)	0.57	518.1
D_3 (0.9 V)	0.527	604.5
D_4 (1.1 V)	0.235	235.5
D_5 (1.3 V)	0.149	25.5
(b)		
T_1 (523 K)	0.445	824
T_2 (548 K)	0.873	2250
T_3 (573 K)	0.573	2078
T_4 (598 K)	0.825	6000
T_5 (623 K)	0.3375	466
T_6 (673K)	1	1369.86

$$2Cu_2O + 2O_2 \xrightarrow{\Delta} 4CuO + O_2 \uparrow$$

Structural and morphological characterizations

Copper oxide can exist in two crystalline phases i.e., cuprous oxide or cuprite (Cu_2O) and cupric oxide or tenorite (CuO) [30]. Both these materials are semiconductors having band gap energy of 1.21–1.51 eV and 2.10–2.60 eV, respectively [31, 32].

Figure 1a shows the XRD patterns of pure Cu (Do) and as-deposited $Cu(OH)_2$ samples at various anodic potentials (D_1, D_2, D_3, D_4, and D_5). Here, it is observed that all samples show crystalline behavior. Sample Do shows orientations along (111), (200), and (220) planes. Value of interplanner spacing 'd' for highly oriented (200) plane is 2.12 Å, while for (111) plane is 2.087 Å. and for (220) plane it is 1.278 Å. The observed 'd' values properly matches with standard 'd' values taken from JCPDS data card no.85-1326 for pure Cu showing cubic crystal structure and JCPDS data card no. 72-0140 for $Cu(OH)_2$ showing orthorhombic crystal structure.

The optimized sample D_3 gets annealed in air for 1 h by varying the temperatures from 523 to 673 K by the interval of 25 K. The annealed samples are denoted as T_1, T_2, T_3, T_4, T_5, and T_6. Figure 1b shows XRD patterns of these samples. Here, it is observed that all samples show crystalline behavior. The observed 'd' values properly match with standard 'd' values taken from JCPDS data card no.44-0706 exhibiting monoclinic crystal structure for CuO and for JCPDS data card no.74-1230, exhibiting cubic crystal structure for Cu_2O. At lower annealing temperatures, from 523 to 598 K (samples T_1 to T_4), the oxidation occurs at the top surface and Cu_2O grows down to the lower layer so that only Cu_2O

Table 2 Variations of SE, SP, and η with applied current densities of T_4 electrode

Current density (mA/cm^2)	SE (Wh/kg)	SP (KW/kg)	η (%)
1	5.46	1.2657	89.51
2	4.62	2.571	93.65
3	4.82	3.857	86.12
4	4.25	5.142	91.41
5	3.96	6.428	94.11
6	3.66	7.714	97.15

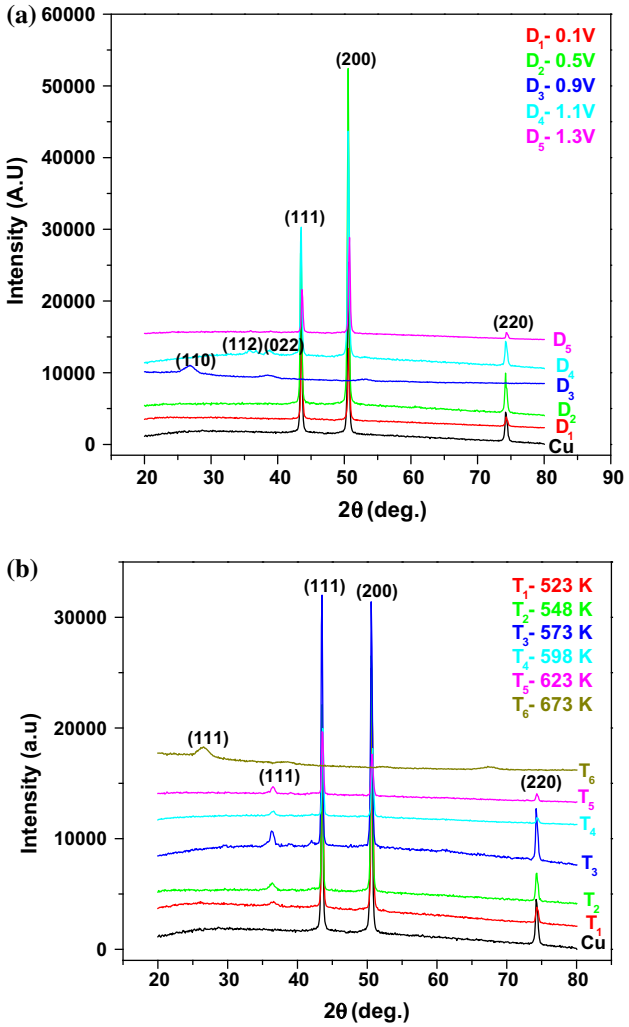

Figure 1 **a** The XRD patterns of as deposited $Cu(OH)_2$ samples as a function of deposition potential **b** the effect of annealing temperature on $Cu(OH)_2$ samples deposited at 0.9 V and for 30 min.

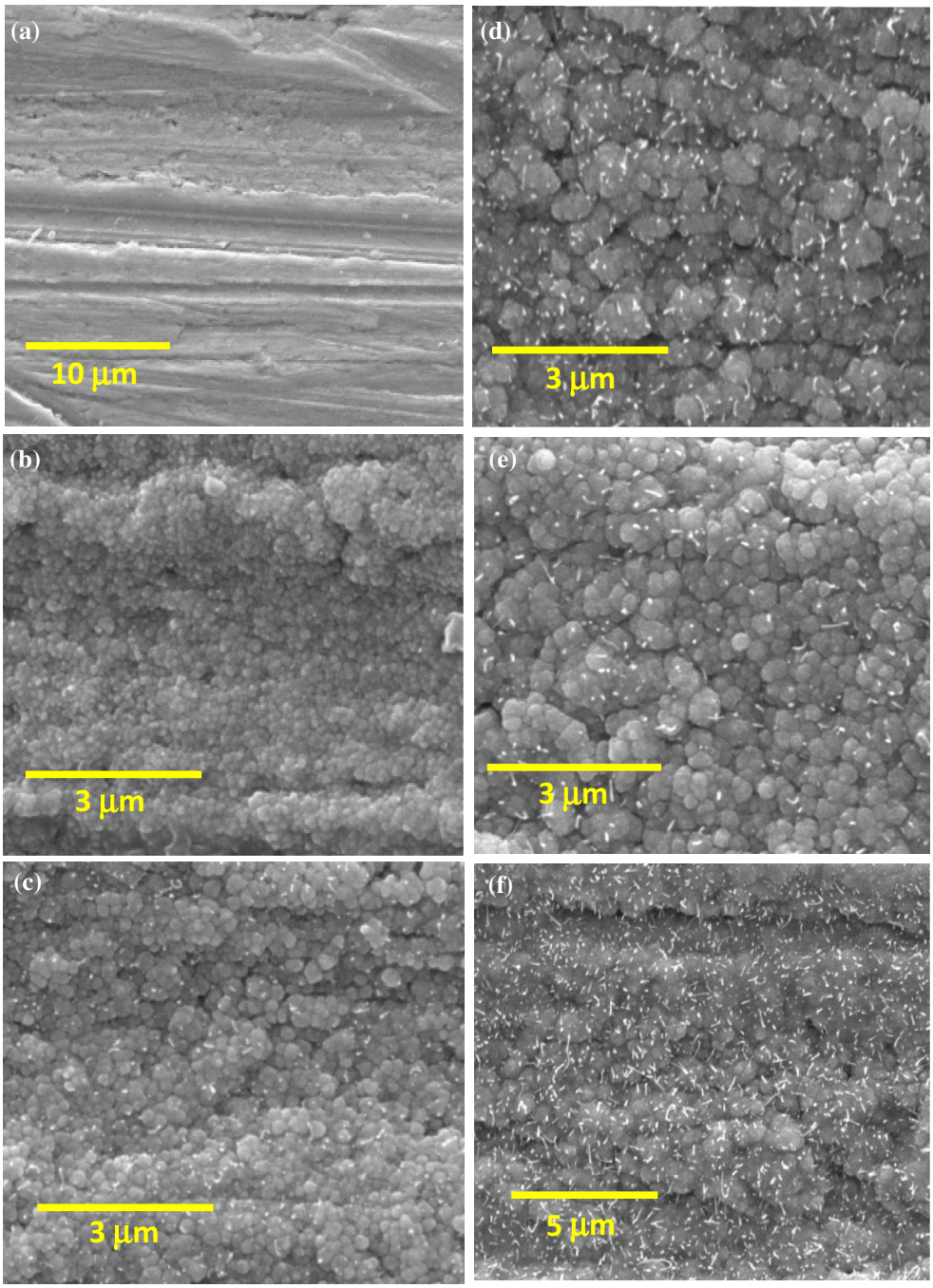

Figure 2 **a** SEM images for as deposited $Cu(OH)_2$ sample and the effect of annealing temperatures **b** 523 K, **c** 548 K, **d** 573 K, **e** 598 K, **f** 623 K on $Cu(OH)_2$.

(111) is able to form [33]. As temperature increases to 673 K (sample T_6), the phase transformation was observed and the mixture of CuO and Cu_2O phases is obtained due to the change in +2 oxidation state to +1 oxidation state and vice versa [28].The oxidation process promotes the phase transformation from pure cubic Cu to cubic Cu_2O to cubic-monoclinic Cu_2O–CuO mixed phase [34]. The value of crystallite size 'D' was calculated for predominant (111) plane using Scherer's formula [35].

$$D = \frac{0.9\lambda}{\beta \cos\theta} \quad (1)$$

where 0.9 is the Scherer's constant, 'λ' is the wavelength of X-ray, 'β' is the full-width at half maximum, and 'θ' is the diffraction angle. With increase in annealing temperature from T_1 to T_6, the average

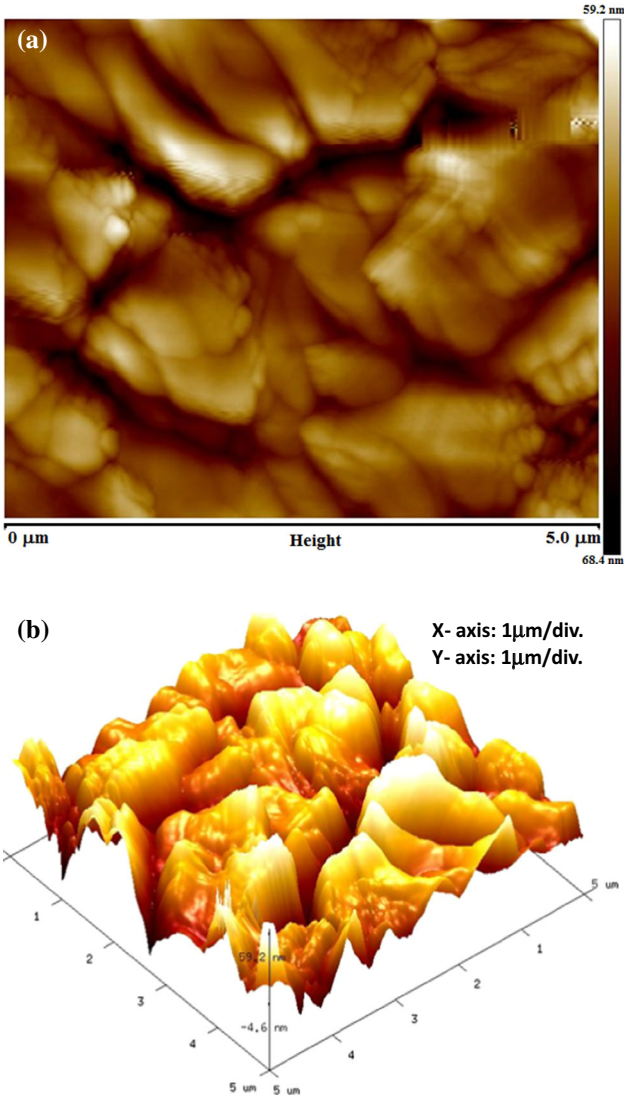

Figure 3 **a** 2D and **b** 3D AFM images of $Cu(OH)_2$ sample deposited at 0.9 V, 30 min, and annealed at 598 K.

crystallite size D increases from 31.029 to 44.04 nm. The increase in crystallite size can be attributed due to the change in crystallographic phase from Cu_2O to CuO [35]. The relative intensity of (111) peak for T_4 is high as compare to other electrodes that may be due to better crystalline nature of the Cu_2O.

Figure 2 shows scanning electron micrographs (SEM) of different samples. Figure 2a shows dense surfaces for hydroxide thin film (sample D_3), while copper (I) oxide (Fig. 2b–f) shows uniformly distributed rough granular type of morphology. With increase in the annealing temperature from 523 to 598 K, the increase in granular size was clearly observed which may facilitate the increase in active surface area of the copper oxide and hence may useful in improvement of the electrochemical performance of the copper oxide thin film samples. With further increase in temperature to 623 K, grains merge together forming mud-like compact surfaces. The grain size increases from 130 to 833 nm from sample (b) to (f), respectively. AFM scanning of the optimized T_4 sample was made to study surface topography and roughness of the films. The 2D and 3D images of AFM scanning are shown in Fig. 3a, b, respectively. For measuring the surface roughness of the films, $4.39 \times 4.24\ \mu m^2$ area was utilized. The roughness of the sample is observed to be 125 nm. Weight loss of the deposited material with annealing temperature is demonstrated in Fig. 4 deposited mass (for T_1-0.0028 gm) continuously deceases with increase in temperatures (for T_2-0.0024 gm, T_3-0.0016 gm, T_4-0.0008 gm), the observed loss in mass may be due to desorption of the physisorbed water molecules [29]. For T_5 and T_6, no much loss is observed.

Electrochemical characterizations

The electrochemical performance of all copper hydroxide and copper oxide samples was studied by using three-electrode cell containing 1 M aqueous NaOH solution. Cyclic voltammetry (CV) characterization was carried within potential windows −0.6 to +0.2 V for $Cu(OH)_2$ and −0.7 to +0.2 V for Cu_2O/CuO electrodes at 2 mV/s. CV curves of $Cu(OH)_2$ and Cu_2O/CuO shows large current, small potential window, large area under curve, and also asymmetric nature having larger tail of reduction. It may be due to the electrochemical reduction reaction of $Cu(OH)_2$ and Cu_2O/CuO with Na^+ ions and the formation of solid electrolyte interface (SEI) films [36].

For the samples D_1 to D_5 (Fig. 5a), the main cathodic peak was observed for all deposition potentials. For the sample D_1, reduction peak was observed at −0.18 V with small oxidation peak, while reduction peak gets shifted to right at −0.13 V for D_2 sample. This shifting of peak occurs due to the presence of some irreversible processes in the electrode material [16]. For sample D_3, the reduction peak was observed at −0.15 V with little large anodic peak than D_1 and D_2 samples, which gives good reversibility of the electrochemical reaction [21]. Hence the value of SC was maximum for D_3 sample

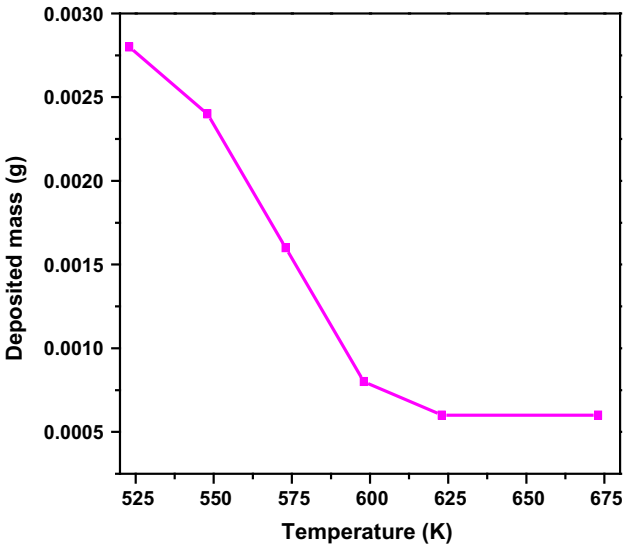

Figure 4 Deposited mass versus temperature curve for Cu $(OH)_2$ samples carried at 0.9 V, for 30 min at different annealing temperatures.

i.e., 604.5 F/g at 2 mV/s. For sample D_4 and D_5, reduction peak shifted towards −0.18 V with a small oxidation peak and with small area under the curve. The pseudocapacitance of copper oxide electrode is the result of transition between +2 and +1 oxidation state and vice versa [28, 35]. The capacitance (C) and specific capacitance (SC) values of the samples carried at different deposition potentials are tabulated in Table 1a.

Figure 5b shows the CV curves of sample T_1 to T_6 carried at different temperatures exhibiting asymmetric nature of the curves. The reduction peaks of all the samples T_1 to T_6 were observed at −0.1 V with small oxidation peak. For sample T_4, the area under curve increases with large oxidation peak. Hence the T_4 sample gives maximum value of SC i.e., 6000 F/g at 2 mV/s. Samples from T_1 to T_5 show stable phase of Cu_2O, while Cu_2O–CuO mixed phase was observed for sample T_6. Which may be the reason for further decrease in the electrochemical performance and hence the SC values of T_6 sample. The values of C and SC for all the samples annealed at different temperatures are tabulated in Table 1b. The values of C and SC associated with electrode were calculated from the following relations.

$$C = \frac{I}{dv/dt} \tag{2}$$

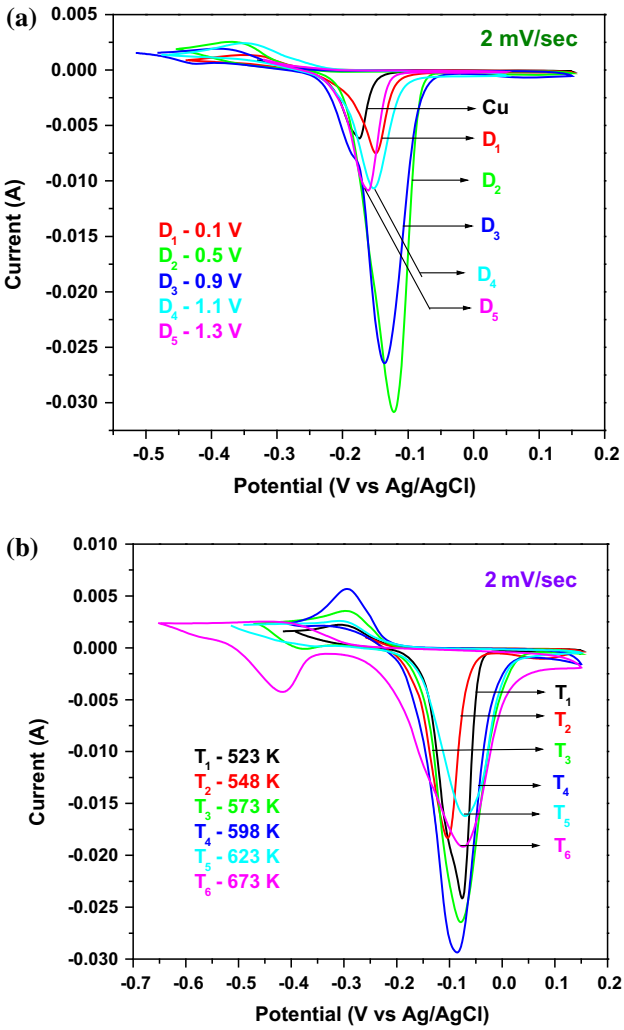

Figure 5 **a** CV curves of as deposited $Cu(OH)_2$ samples and **b** CV curves of annealed $Cu(OH)_2$ samples at 2 mV/s in 1 M NaOH.

$$SC = C/W \tag{3}$$

where I is the average current, dv/dt is the voltage scan rate, C is the capacitance, SC is the specific capacitance, W is the weight of the material dipped in electrolyte. Charge–discharge variation of the annealed Cu_2O electrodes was observed at different current densities in 1 M NaOH. Figure 6a shows charge–discharge variation of optimized T_4 electrode scanned within potential window −0.6 to 0.2 V for variable current densities 1–6 mA/cm^2. The non-symmetrical discharging behavior was observed at all current densities, which clearly indicates the pseudocapacitive behavior of the Cu_2O thin film samples. In discharging curve, a sudden voltage drop (linear part parallel to Y-axis) represents a voltage

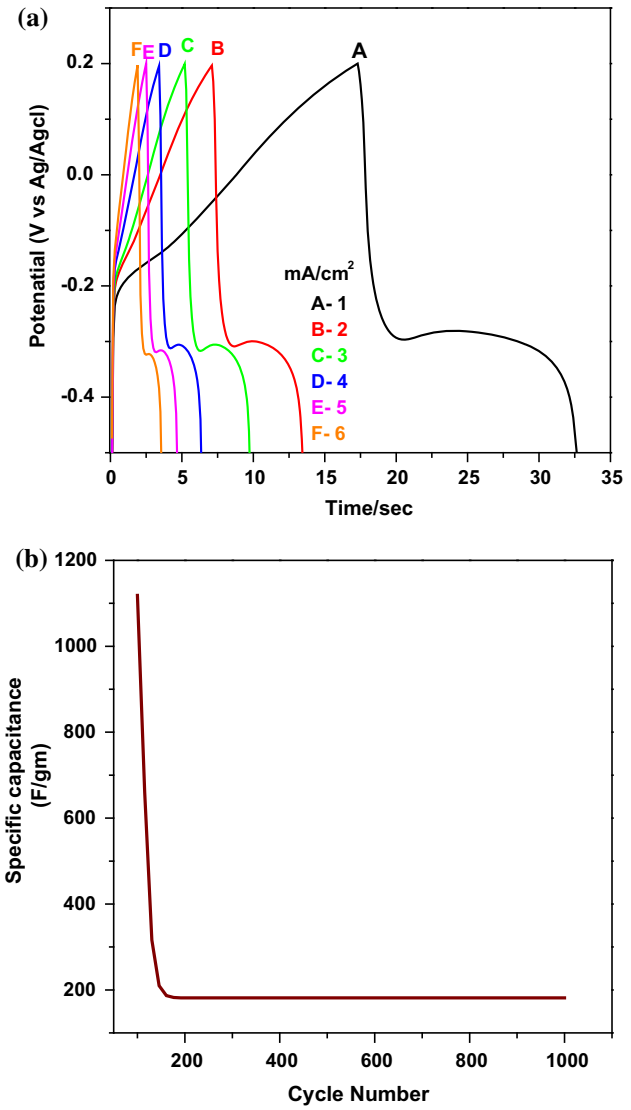

Figure 6 **a** Charge–discharge study and **b** stability curve of $Cu(OH)_2$ sample deposited at 0.9 V, 30 min, and annealed at 598 K.

change due to change in internal resistance and a capacitive component related to the voltage change [25]. The electrical parameters such as specific energy (SE), specific power (SP), and columbic efficiency (η) were calculated from discharging curves using the relations [37, 38].

$$\mathrm{SE} = \frac{V \times Id \times td}{W} \tag{4}$$

$$\mathrm{SP} = \frac{V \times Id}{W} \tag{5}$$

$$\eta = \frac{td}{tc} \times 100 \tag{6}$$

where V is the voltage, Id and td are the discharging current and time, respectively, W is the weight of the material dipped in electrolyte, and tc is the charging time. The values of SE, SP, and η are summarized in Table 2.

Electrochemical stability (Fig. 6b) of optimized T_4 electrode was measured in 1 M NaOH at 100 mV/s for 1000 CV cycles. The observed capacity retention of 26 % just within 200 cycles indicates poor stability of the Cu_2O thin films. This may be due to slight phase change from $Cu(OH)_2$ to CuO through intermediate stage of Cu_2O which might cause collapse of its intrinsic lattice structure and show diminution of its capacitance [39].

Electrochemical impedance measurements were made to search internal resistance of the electrode. Figure 7a shows the Nyquist plot between real and imaginary impedance values in the frequency range of 1 mHz–1 MHz, obtained at −0.249 V open circuit potential. At high frequency region, the crossover point of the highest frequency with the real part of the impedance is in general a net resistance of the electrolyte, intrinsic resistance of substrate, and contact resistance between the active material and the current collector. The observed internal resistance is ~1.75 Ω/cm^2. In the intermediate region of the frequency, the straight line nature with the inclination of ~45° to the real axis was noticed, which in fact the characteristic of ion diffusion into the electrode materials [2]. In the low frequency range, the straight line part was leaned slowly toward the imaginary axis, indicating that the electrode material experiences capacitive behavior [40]. Figure 7b (Nyquist plot of Z″ vs Z′) shows the experimental and standard curves obtained by simulation using ZsimpWin software, and the inset in this figure shows matched equivalent circuit. Evaluated circuitry parameters are as follows: $R_1 = 1.851\ \Omega$, $R_2 = 1.883\ \Omega$, $R_3 = 22.03\ \Omega$, and $R_4 = 0.05909\ \Omega$ are the charge transfer resistances, and $C_1 = 4.994 \times 10^{-5}$ F is the capacitance with $Q = 0.009036$ and Warburg impedance $(W) = 0.03471$.

Conclusion

Copper hydroxide thin films were successfully obtained by using the anodization of the copper substrate at different deposition potentials. The as-

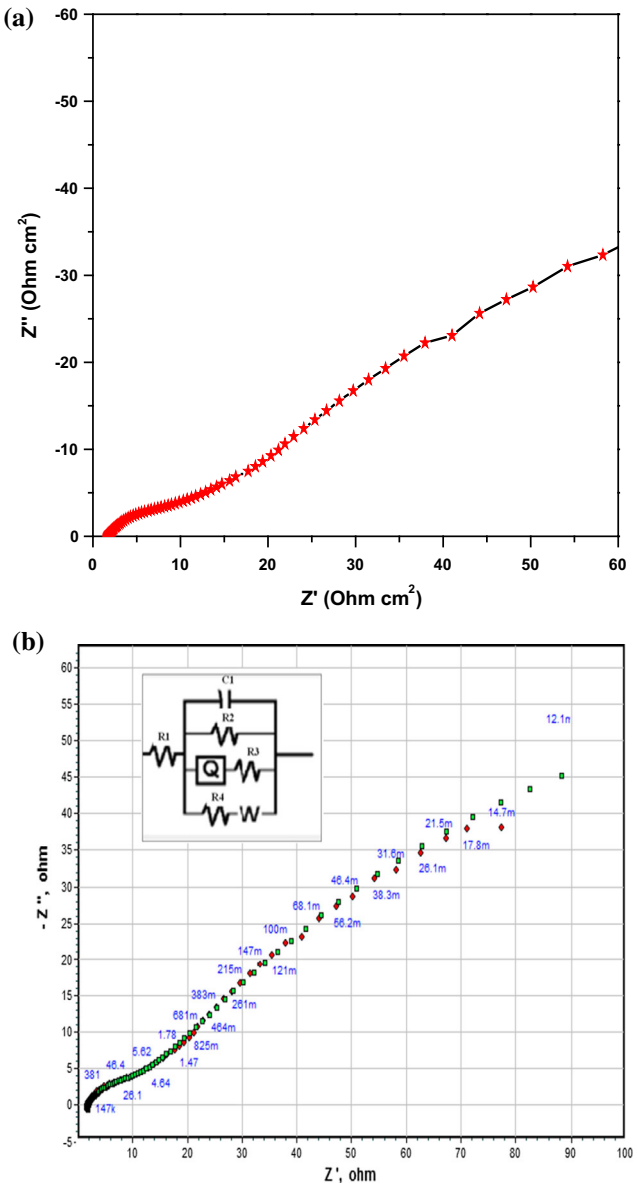

Figure 7 **a** Nyquist plot and **b** matched equivalent circuit of $Cu(OH)_2$ sample deposited at 0.9 V, 30 min, and annealed at 598 K.

deposited copper hydroxide samples $Cu(OH)_2$ reveal orthorhombic crystal structure, whereas the cubic Cu_2O phase changes to cubic-monoclinic Cu_2O–CuO mixed phase due to the post annealing treatment at higher temperature. SEM images depict rough and uniformly distributed granular type of morphology; increase in annealing temperature affected granular size. The Cu_2O electrode (T_4) exhibits maximum SC of 6000 F/g at 2 mV/s, with SE 5.46 Wh/kg, SP 7.714 KW/kg and η 97.15 %. The stability study shows 26 % capacitive retention. Observed internal resistance from the Nyquist plot is about 1.75 Ω/cm^2. The overall study indicates that the excellent capacitive performance of the Cu_2O electrode will be suitable for energy and power applications in supercapacitor technology by overcoming the stability problem observed during the study.

Acknowledgements

The authors thank the DST-SERB for providing financial support through the project scheme 2014/DST-SERB/4688.

References

[1] Meher SK, Justin P, Rao GR (2010) Pine-cone morphology and pseudocapacitive behavior of nanoporous nickel oxide. Electrochim Acta 55:8388

[2] Lokhande BJ, Ambare RC, Mane RS, Bhardwaj SR (2013) Concentration-dependant electrochemical supercapacitive performance of Fe_2O_3. Curr Appl Phys 6:985

[3] Conway BE (1999) Electrochemical supercapacitors: scientific fundamentals and technological applications. Kluwer-Plenum, New York

[4] Reddy ALM, Ramaprabhu S (2007) Nanocrystalline metal oxides dispersed multiwalled carbon nanotubes as supercapacitor electrodes. J Phys Chem C 111:7727

[5] Ishikawa M, Morita M, Ihara M, Matsuda Y (1994) Electric double-layer capacitor composed of activated carbon fiber cloth electrodes and solid polymer electrolytes containing alkyl ammonium salts. J Electrochem Soc 141:1730

[6] Mayer ST, Pekala RW, Kaschmitter JL (1993) The aerocapacitor: an electrochemical double-layer energy storage device. J Electrochem Soc 140:446

[7] Prasad KR, Munichandraian N (2002) Potentiodynamically deposited polyaniline on stainless steel inexpensive, high-performance electrodes for electrochemical supercapacitors. J Electrochem Soc 149:A1393

[8] Mitra S, Shukla AK, Sampath S (2001) Electrochemical capacitors with plasticized gel-polymer electrolytes. J Power Sources 101:213

[9] Hu CC, Huang YH (1999) Cyclic voltammetric deposition of hydrous ruthenium oxide for electrochemical capacitors. J Electrochem Soc 146:2465

[10] Chen WC, Hu CC, Wang CC, Min CK (2004) Electrochemical characterization of activated carbon–ruthenium oxide nanoparticles composites for supercapacitors. J Power Sources 125:292

[11] Zheng JP, Cygan PJ, Jow TR (1995) Hydrous ruthenium oxide as an electrode material for electrochemical capacitors. J Electrochem Soc 142:2699

[12] Park BO, Lokhande CD, Park HS, Jung KD, Joo OS (2004) Electrodeposited ruthenium oxide (RuO_2) films for electrochemical supercapacitors. J Mater Sci 39:4313. doi:10.1023/B:JMSC.0000033415.47096.db

[13] Wang D, Wang Q, Wang T (2011) Controlled synthesis of mesoporous hematite nanostructures and their application as electrochemical capacitor electrodes. Nanotechnology 22:135604

[14] Zhu J, Sharma YK, Zeng Z, Zhang X, Shrinivasan M, Mhaisalkar S, Zhang H, Hng HH, Yan QJ (2011) Cobalt oxide nanowall arrays on reduced graphene oxide sheets with controlled phase, grain size, and porosity for Li-ion battery electrodes. Phys Chem 115:8400

[15] Kore RM, Mane RS, Naushad M, Khan MR, Lokhande BJ (2016) Nanomorphology-dependent pseudocapacitive properties of NiO electrodes engineered through a controlled potentiodynamic electrodeposition process. RSC Adv 6:24478

[16] Han DD, Jing XY, Wang J, Yang PP, Song DL, Liu JY (2012) Porous lanthanum doped NiO microspheres for supercapacitor application. J Electroanal Chem 682:37

[17] Sun Y, Hu X, Luo W, Huang Y (2011) Self-assembled hierarchical MoO_2/graphene nanoarchitectures and their application as a high-performance anode material for lithium-ion batteries. ACS Nano 5:7100

[18] Zhang YX, Zhu SJ, Dong M, Liu CP, Wen ZQ (2013) Hydrothermally tailoring low-dimensional MnOx nanostructure and their high electrochemical performance. Int J Electrochem Sci 8:2407

[19] Xiao Y, Zhang Q, Yan J, Wei T, Fan Z, Wei F (2012) Compressible aligned carbon nanotube/MnO_2 as high-rate electrode materials for supercapacitors. J Electroanal Chem 4:32

[20] Ko S, Lee J, Yang HS, Park S, Jeong U (2012) Mesoporous CuO particles threaded with CNTs for high-performance lithium-ion battery anodes. Adv Mater 24:4451

[21] Wang G, Huang J, Chen S, Gao Y, CaO D (2011) Preparation and supercapacitance of CuO nanosheet arrays grown on nickel foam. J Power Sources 196:5756

[22] Shrestha NK, Yoon SJ, Lee M, Lee DY, Lim I, Mane RS, Sung MM, Han SH (2011) Self-organized growth of magnetic nanoporous thin film by alloy anodization. Microporous Mesoporous Mater 144:200

[23] Wu X, Bai H, Zhang J, Chen F, Shi G (2005) Copper hydroxide nanoneedle and nanotube arrays fabricated by anodization of copper. J Phys Chem B 109:22836

[24] Park SH, Kim HJ (2004) Unidirectionally aligned copper hydroxide crystalline nanorods from two-dimensional copper hydroxy nitrate. J Am Chem Soc 126:14368

[25] Jadhav VV, Shinde DV, Patil SA, Zate MK, Pawar S, Al-Osta A, Mane RS, Han SH (2014) Electrochemical properties of anodized copper hydroxide nanostructures. J Nanoeng Nanomanufacturing 4:1

[26] Zhang WX, Wen XG, Yang SH, Betra Y, Wang ZL (2003) Single crystalline scroll-type nanotube arrays of copper hydroxide synthesized at room temperature. Adv Mater 15:822

[27] Wen XG, Zhang WX, Yang SH (2003) Synthesis of $Cu(OH)_2$ and CuO nanoribbon arrays on a copper surface. Langmuir 19:5898

[28] Patake VD, Joshi SS, Lokhande CD, Joo OS (2009) Electrodeposited porous and amorphous copper oxide film for application in supercapacitor. Mater Chem Phys 114:6

[29] Shaikh JS, Pawar RC, Moholkar AV, Kim JH, Patil PS (2011) CuO–PAA hybrid films: chemical synthesis and supercapacitor behavior. Appl Surf Sci 257:4389

[30] Johan MR, MohdSuan MS, Hawari NL, Ching HA (2011) Annealing effects on the properties of copper oxide thin films prepared by chemical deposition. Int J Electrochem Sci 6:6094

[31] Yoon KH, Choi WJ, Kang DH (2000) Photoelectrochemical properties of copper oxide thin films coated on an n-Si substrate. J Thin solid films 372:250

[32] Oral AY, Mensur E, Aslan MH, Basaran E (2004) The preparation of copper(II) oxide thin films and the study of their microstructures and optical properties. Mater Chem Phys 83:140

[33] Qiang LJ, Xia MZ, Qian YD, Nan HY, Ping LY, Kuznotsov AY, Long DX (2012) Temperature dependence of Cu_2O orientations in oxidation of Cu (111)/ZnO (0001) by oxygen plasma. Chin Phys B 21:076401

[34] Han S, Chen HY, Chu YB, Shih HC (2005) Phase transformation in copper oxide nanowires. Am Vac Soc 23: 2558

[35] Cullity BD (1978) Elements of X-ray diffraction, 2nd edn. Addison-Wesley Publishing Company, Reading, p 284

[36] Yang X, Fan K, Zhu Y, Shen J, Jiang X, Zhao P, Luan S, Li C (2013) Electric papers of graphene-coated Co_3O_4 fibers for high performance lithium-ion batteries. ACS Appl Mater Interfaces 5:997

[37] Ambare RC, Bharadwaj SR, Lokhande BJ (2013) Concentration and volume of the spraying solution affects on the capacitive behaviour of the Co_3O_4 thin films. Int J Renew Energy 3:212

[38] Koneshan S, Rasaiah JC, Lynden-Bell RM, Lee SH (1998) Solvent structure, dynamics and ion mobility in aqueous solutions at 25 °C. J Phys Chem B 102:4193

[39] Chang J, Park M, Ham D, Ogale SB, Mane RS, Han SH (2008) Liquid-phase synthesized mesoporous electrochemical supercapacitors of nickel hydroxide. Electrochim Acta 53:5016

[40] Yan J, Wei T, Qiao WM, Shao B, Zhao QK, Zhang LJ, Fan ZJ (2010) Rapid macrowave assisted synthesis of grapheme nanosheet/Co_3O_4 composite for supercapacitor. Electrochem Acta 55:6973